

Adsorption of heavy metal ions from aqueous solutions using metal organic frameworks: kinetic and thermodynamic study

Somayeh Tourani^{a,*}, Alireza Behvandi^a, Abolghasem Aghajari^a, Nasrin Aghajari^b

^aDepartment of Chemical Engineering, Mahshahr branch, Islamic Azad University, Mahshahr, Iran, Postal Code: 63518-24859, ORCID: 0000-0003-3462-1545, emails: s.tourani@mhriau.ac.ir (S. Tourani), behvandi.chemeng@gmail.com (A. Behvandi), aghajari.a1982@gmail.com (A. Aghajari)

^bDepartment of Environmental Science, Faculty of Natural Resources, Tarbiat Modares University, Noor, Iran, email: nasrinaghajari70@gmail.com

Received 25 August 2018; Accepted 23 February 2019

ABSTRACT

In this work, metal-organic-frameworks were employed as adsorbents to remove cobalt and manganese from aqueous solutions. In order to achieve this goal, the MIL-53(Al), MIL-101(Cr), and Cu-BTC were synthesized by hydrothermal method. The adsorbents were characterized by Brunauer–Emmett–Teller analysis, Fourier transform infrared, X-ray diffraction, transmission electron microscopy, scanning electron microscopy, differential thermal analysis, and thermogravimetric analysis. After that, MIL-101(Cr) as the proper adsorbent was modified by ethylenediamine at different concentrations of 2, 5, and 10 mmol. MIL-101-5 was shown to possess excellent performance which is more than two times as that of MIL-101(Cr). The effects of varying parameters such as pH, temperature, initial metal concentration, and contact time on the adsorption process were examined. The adsorption kinetics was fitted well with a pseudo-second-order model and the adsorption data correlated with Langmuir, Freundlich, Temkin, and Redlich–Peterson isotherms. Finally, the Langmuir isotherm was found to fit the equilibrium data. The thermodynamic study showed that the adsorption process was a spontaneous and exothermic process because of negative values of ΔG and ΔH at all temperatures. The most desired parameters in the adsorption process were as follows: adsorption equilibrium time of about 90 min, the maximum adsorption of ions on the MIL-101-ED-5 was observed to occur at pH = 6.5, and the Co and Mn concentration of 30 mg L⁻¹. The efficiency of cobalt and manganese at these conditions was identified as 90.32% and 87.33%, respectively.

Keywords: Cobalt; Manganese; MOFs adsorbent; Ethylenediamine

1. Introduction

Different industrial wastewaters containing heavy metals frequently pollute the aquatic streams. The presence of these heavy metals in the environment is one of the important concerns due to their toxicity and health effects on the humans and other living creatures [1,2]. Therefore, elimination of toxic metals is attended by many researchers. There are various methods for removing of heavy metals

from aqueous streams such as chemical precipitation [3,4], reverse osmosis [5,6], ion-exchange resins [1,3], coagulation [7,8], adsorption [9,10], electrochemical methods [11,12], and wastewater stabilization through cementation [13] were used by many researchers. Adsorption of heavy metals by adsorbents is a physicochemical process, which is used extensively as an effective and economic method [2,14,15]. Moreover, various types of adsorbents were utilized for the adsorption of heavy metals from waste solution such as

* Corresponding author.

aluminum salts, aluminum oxide, iron oxide, zeolite, clay, and micro-cavity materials [6,16]. Metal organic frameworks (MOFs) are a class of crystalline porous nanomaterial composed of metal ions (or clusters) and coordinating linkers which impart high porosity to the MOFs structures. The particular interest in MOF materials for various purposes such as adsorption is due to the easy tunability of their pore size and shape from a microporous to a mesoporous scale, by changing the connectivity of the inorganic moiety and the nature of the organic linkers [17,18]. MOF compounds help create a structure with designing, organizing, and flexibility capacity in order to create unique properties such as high mechanical and thermal sustainability, low density, very high porosity, high specific area, and higher adsorption capacity, compared with other known adsorbents [18,19]. During the past years, a large number of studies have been conducted in the field of adsorption and storage from the gas phase, catalytic applications, sensors, and isomer separation by MOFs [20]. However, few studies were conducted in the field of adsorption from the liquid phase, especially industrial wastewater [21]. In the present work, we have focused on the removal of cobalt and manganese ions from aqueous solutions using MOFs. For this purpose, Cu-BTC, MIL-101(Cr), and MIL-53(Al) were synthesized, characterized, and used as adsorbent materials for the removal of Co and Mn from aqueous media. The results were compared with the commercial activated carbon (AC) adsorbent. Moreover, the effect of some important parameters such as pH, contact time, the initial concentration of cobalt and manganese and temperature was investigated. Also the adsorption kinetics, isotherm models, and thermodynamics of Co and Mn adsorption process are evaluated.

2. Experimental

2.1. Adsorbents synthesis and characterization

2.1.1. Synthesis of Cu-BTC (HKUST-1)

First, 9 mmol of benzenetricarboxylic acid (BTC) is added to 20 mL of ethanol, the resulted mixture is stirred until the BTC is totally dissolved (first mixture). Then, 10 mL of deionized water is solved in 18 mmol copper nitrate-trihydrate (second mixture). After that, the first and second mixtures are combined and stirred for 16 h under the environmental temperature. The mixture is then transferred into a 50 mL Teflon-lined autoclave reactor for hydrothermal treatment at 140°C for 48 h. Then, after filtration, it is washed with deionized water several times. Finally, the obtained aqueous crystals are placed in an oven at 85°C and are dried under vacuum condition for 16 h [22].

2.1.2. Synthesis of MIL-101(Cr)

MIL-101(Cr) was prepared by 5 mmol chromium nitrate and 5 mmol of terephthalic acid are combined with 25 mL of deionized water and placed under magnetic stirring for 30 min. Meanwhile, 0.25 mL HF was added to this solution. For the better uniformity, the mixture was placed under ultrasonic stirring for 15 min. In the next step, the obtained mixture was put in a 15 mL Teflon-lined autoclave reactor and placed in a thermal furnace at 220°C for 8 h. After the filtration, the crystallized unreacted terephthalic acid and

green crystals of MIL-101(Cr) separated from the mother liquor by Büchner funnel. In order to remove the unreacted terephthalic acid molecules from the structure of synthesized MIL-101(Cr), the obtained solid product was added to 30 mL of dimethyl formaldehyde (DMF) and placed under the stirring at 70°C for 8 h. It should be mentioned that this step was repeated twice. After filtration, the product was rewashed and filtered again under stirring with 30 mL of dried ethanol for 8 h. Finally, the purified MIL-101(Cr) was placed on the oven at 150°C for 24 h and accordingly the obtained green powder product was kept in desiccator in order to avoid absorbing moisture [23].

2.1.3. Synthesis of MIL-53(Al)

17.5 mmol of aluminum nitrate and 75.8 mmol of terephthalic acid were added to 25 mL of deionized water and the resulted solution was mixed for 30 min. Then, the obtained mixture was placed under ultrasonic stirring for 15 min for better homogeneity. In the next stage, the mixture was stirred under a 50 mL stainless steel Teflon-lined reactor and placed under a thermal furnace at 220°C for 72 h. After filtering the contents of the reactor, the obtained cream powder was washed with water. The process was continued until the pH of filtered fluid reaches approximately 7. Next, the obtained powder was added to 30 mL of DMF and was placed under stirring at 70°C for 8 h in order to remove the unreacted terephthalic acid. This process was repeated twice. After more filtration, the washing process was continued by using the dried ethanol in order to remove DMF and extra water from MIL-53(Al) structure. Finally, the obtained cream powder was kept and dried in desiccator to prevent it from absorbing moisture for 16 h under vacuum at 85°C [23,24].

2.1.4. Activated carbon

The employed AC for this study was purchased from the Duksan Pure Chemicals (South Korea). The characteristics of AC are shown in Table 1.

2.1.5. Functionalization of MIL-101 by ethylenediamine

Functionalization of MIL-101 (Cr) crystals was done with following procedure reported by Luo et al. [25]. Typically, 1 g of synthesized adsorbent (MIL-101) was dehydrated in an oven for 12 h at 150°C under vacuum in order to produce coordinately unsaturated sites. After suspending the sample into 75 mL of toluene, an appropriate amount of ethylenediamine solution (136 μ L for 2 mmol, 340 μ L for 5 mmol, and 680 μ L for 10 mmol functionalization) was added to the mixture and reacted for 12 h. Eventually, the final sample was collected through filtration and washing with a large amount of ethanol and dried for 24 h under the room temperature [25].

2.2. Adsorbents characterization techniques

The morphology of the prepared adsorbents was investigated by transmission electron microscopy (TEM) images that were taken at 80 kV by a JEM 1230 (JEOL Corp., Japan) and SEM measurements were performed by

Table 1
Characteristics of activated carbon

Item	Range
Iodine number	960 mg g ⁻¹
Moisture content	Maximum 1.5%
Total ash content	Maximum 1%
pH	6–7
Bulk density	530 kg m ⁻³
Actual density	1.3–1.4 g cm ⁻³
Hardness	98%
Abrasion	80
Surface area	1,150 m ² g ⁻¹
Particle size	1.1–1.6 mm
Uniformity	1.8

Indian-made Philips scanning electron microscope, XLC30 model, with a voltage of 30 kW electron microscope. Fourier transform infrared (FTIR) spectrum was obtained using Bruker-vector-22 (Germany) with a range of 400–4,000 cm⁻¹. MIL-101(Cr) sample for FTIR analysis was pretreated by grinding the MIL-101(Cr) powder together with KBr in an agate mortar and then by pressing them into flakes by a tablet. The nitrogen adsorption isotherm, Brunauer–Emmett–Teller (BET) surface areas and pore volume of MIL-101(Cr) were measured on a Micromeritics ASAP 2010 sorptometer using N₂ adsorption at 77 K. The BET equation was used to determine the specific surface area and the total pore volume. For these measurements, the powder was degassed and activated under reduced pressure at 105°C for 3 h. In order to identify the phase and the size of the crystal of the synthesized sample, X-ray diffraction (XRD) analysis (Panalytical Corp, The Netherlands) was used. Powder XRD pattern was obtained in an XPert pro diffractometer (Panalytical Corp., The Netherlands) using CuK α radiation. Finally, thermogravimetric analysis (TGA) and differential thermal analysis (DTA), (Mettler Toledo, Australia), were used to study and identify the thermal stability of a material against the heat.

2.3. Adsorption experiments

The adsorption experiments were performed by the batch technique in glass bottles. The initial conditions for all adsorbents are shown in Table 2. The cobalt and manganese concentrations before and after the adsorption experiment were determined by atomic adsorption technique. The pH value of the solutions was adjusted prior to the adsorption experiments by the addition of a small amount of HCl/HNO₃. The adsorption solutions were shaken at the same rate of 100 rpm at various temperatures. At the end of the experiment time, the solution was filtered with a soft paper filter and the filtrate was analyzed to determine the remaining pollutant concentration. The separation percentage of the metal ions and the adsorption capacity of the adsorbents were calculated using the following formulas:

$$\%q_t = \frac{C_0 - C_e}{C_0} \times 100 \quad (1)$$

Table 2
Initial condition of batch adsorption experiment for all studied adsorbents (MIL-101(Cr), MIL-53(Al), Cu-BTC, and carbon active)

Concentration of Co in solution (mg L ⁻¹)	Concentration of Mn in solution (mg L ⁻¹)	Weight of adsorbent (mg)	Volume (ml)
50	50	20	20

$$q_t = \frac{C_0 - C_e}{m} \times v \quad (2)$$

where q_t (mg g⁻¹) is the amount of cobalt and manganese adsorbed at time t (min), C_0 and C_e (mg L⁻¹) are the liquid-phase concentrations of cobalt and manganese at time = 0 and t , respectively, and v (L) and m (g) are the volume of the solution and the mass of the adsorbent, respectively [26,27].

3. Results and discussion

3.1. Adsorbents characterization

The X-ray diffraction patterns of Cu-BTC, MIL-101(Cr), and MIL-53(Al) are presented in Fig. 1a. As shown in Fig. 1a, the XRD patterns of the diffraction peak of all the three synthesized adsorbents include main peaks in the range of 2°–20° [28]. The extremely high intensities of the diffraction peaks (2 θ from 3° to 10°) indicated a good crystallinity of MIL-101(Cr) synthesized in this work. The obtained results were well matched with the reports presented by other researchers [17,26,29,30]. Kun Yang et al. [28] found that the most important peaks are within the ranges of 3, 5, 6, and 9, which indicates the proper crystal structure of these MOFs. Two small peaks in the ranges of 2° and 17° are related to the existence of terephthalic acid in the structure of MOFs [28]. As illustrated in Fig. 1b, the Cu-BTC and MIL-101(Cr) adsorbents isotherms are based on type I of IUPAC isotherm, which indicates the microporosity of the mentioned adsorbents. The steep slope of adsorption of this isotherm at low relative pressures is related to the adsorbate entrance to the cavities of micropore adsorbents. Filling the cavities in less p/p_0 areas represents the smaller size of adsorbent cavities. Therefore, it can be concluded that diameter of cavities of Cu-BTC are smaller than MIL-101(Cr). Further, the higher concavity of adsorption diagram in higher pressures indicates the tendency to capillary condensation, multi-layered adsorption. In other words, the increased volume ratio of mesopore in adsorbent, which is observed more in MIL-101(Cr), and particularly in MIL-53(Al), compared with Cu-BTC. Due to the turbulence in high relative pressures, adsorption/desorption isotherm is similar to type IV of IUPAC isotherm representing the mesoporosity of this adsorbent [24]. The BET analysis results are shown in Table 3. According to the table, the average size of the adsorbent cavities was Cu-BTC < MIL-101(Cr) < MIL-53(Al) respectively, and the ratio of micropore volume to the total volume of cavities was Cu-BTC > MIL-101(Cr) > MIL-53(Al), respectively. The obtained results are consistent with the studies and reports presented by other researchers [22,24,31]. The little difference among the results reported

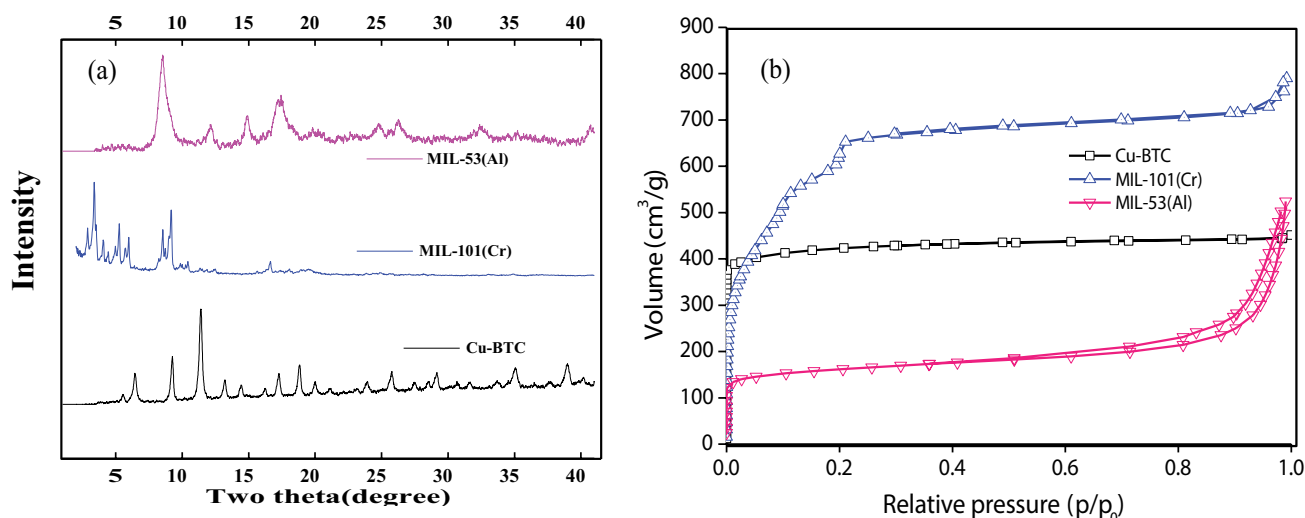


Fig. 1. (a) XRD pattern of synthesized Cu-BTC, MIL-53(Al), and MIL-101(Cr) and (b) BET pattern of synthesized Cu-BTC, MIL-53(Al), and MIL-101(Cr).

Table 3

BET surface area, pore diameter, average pore volume calculated according to the N_2 adsorption isotherms of different adsorbents

Sample	S_{BET} ($m^2 g^{-1}$)	Average pore diameter (nm)	V_{micro} ($m^3 g^{-1}$)	V_{total} ($m^3 g^{-1}$)	V_{micro}/V_{total}
Cu-BTC	1,601	1.73	0.65	0.69	0.94
MIL-101(Cr)	2,390	2.23	0.98	1.32	0.74
MIL-53(Al)	598.2	5.41	0.25	0.81	0.31
Active carbon	1,052	–	–	0.51	–

by researchers is related to the difference in the precision of synthesis, washing, or purification [30,32,33].

The FTIR spectra for Cu-BTC, MIL-101(Cr), and MIL-53(Al) are presented in Fig. 2. The broad and wide band in the ranges of $3,400\text{ cm}^{-1}$ can represent the existence of O–H or N–H band for all compounds. Moreover, the bands available in the range of $1,400$ and $1,550\text{ cm}^{-1}$, indicate a O–C–O vibrational bond, or the existence of carboxylate connector in MIL-53(Al), MIL-101(Cr), Cu-BTC structure [17,28]. The peaks in 750 and $1,020\text{ cm}^{-1}$ are also related to the vibration of benzene rings. The peaks available on the 580 cm^{-1} range of MIL-101(Cr) and MIL-53(Al) structure are related to the existence of –COO bond internally or externally are bonded to adsorbent surface. Peaks of the $2,930$ and $3,130\text{ cm}^{-1}$ wavelengths are related to aromatic C–H tensile band. Regarding the three MOFs, these organic-metal bonds can be observed at $480\text{--}490\text{ cm}^{-1}$ wavelength range [17,25,34].

Scanning electron microscopy (SEM) and TEM images are shown in Figs. 3 and 4, respectively. Figs. 3c and 4c illustrate the tetrahedral crystals of MIL-101(Cr), with an average size of $400\text{--}500\text{ nm}$. Three synthesized MOFs enjoyed a good morphology and crystal structure and the results are in line with the results of other studies [26,31,34].

The TGA and DTA profiles of each synthesized adsorbents are shown in Fig. 5. All synthesized MOFs have a desirable thermal stability. The starting point of the compound structure destruction is the beginning of its intense weight loss in TGA chart, or the beginning of an intense endothermic

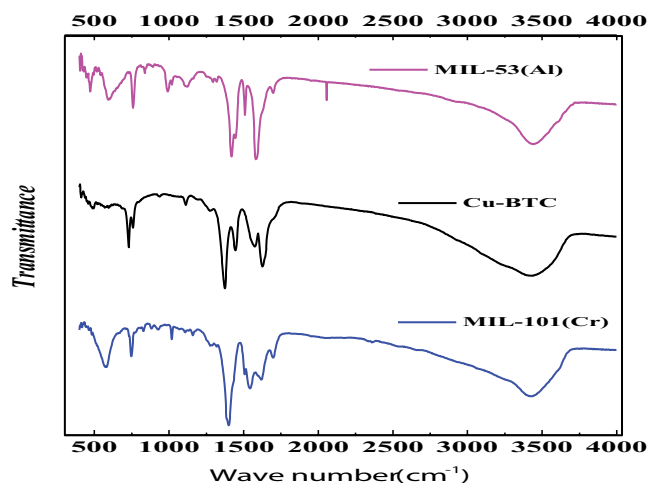


Fig. 2. FTIR spectra of synthesized MIL-53(Al), MIL-101(Cr), and Cu-BTC.

peak in DTA chart. According to the Figs. 5a–c, Cu-BTC, and MIL-53(Al), and MIL-101(Cr) are stable until reaching the temperatures of 350°C , 550°C , and 352°C , respectively. The organic molecules are destructed due to the breakdown of their organic-metal bonds. It should be mentioned that the slight reduction in sample weight or smaller DTA peaks in the range of $80^\circ\text{C}\text{--}100^\circ\text{C}$ is related to the surface evaporation

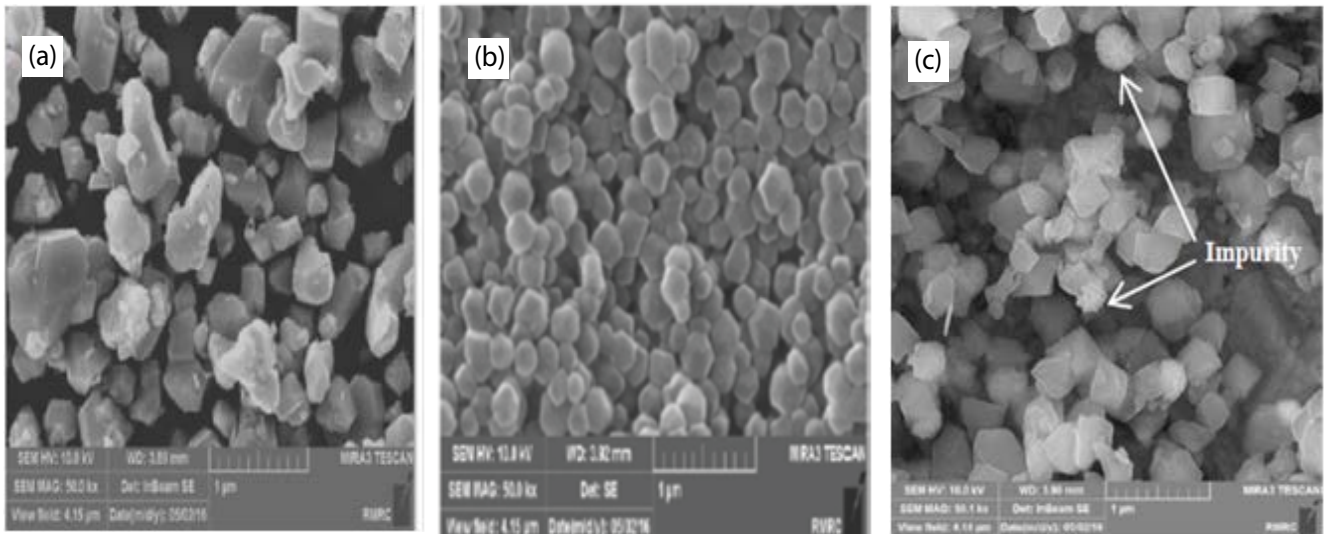


Fig. 3. SEM pattern of synthesized (a) Cu-BTC, (b) MIL-53(Al), and (c) MIL-101(Cr).

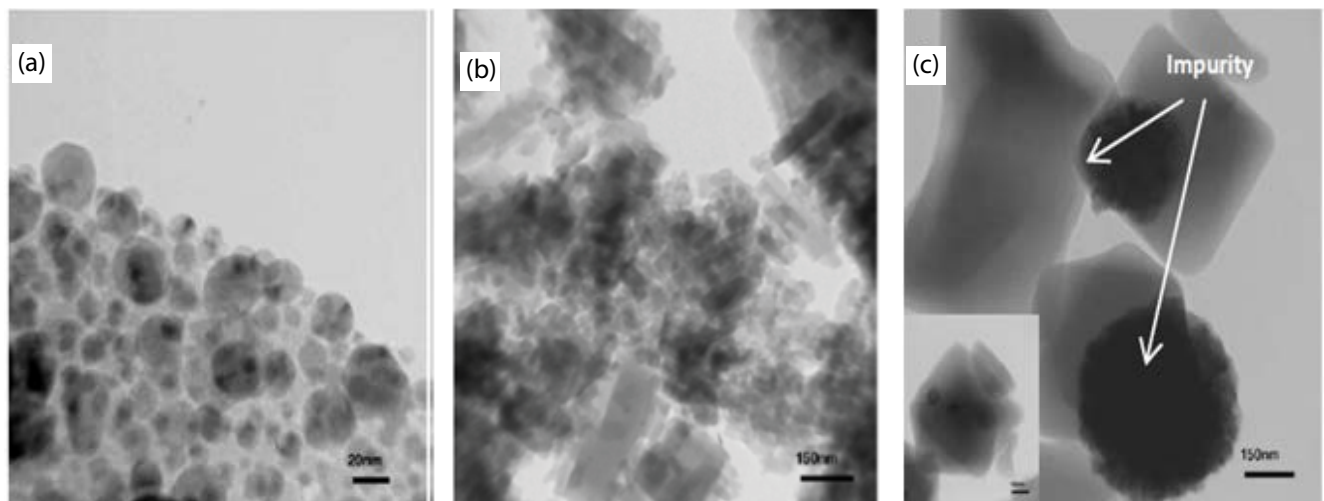


Fig. 4. TEM pattern of synthesized (a) Cu-BTC, (b) MIL-53(Al), and (c) MIL-101(Cr).

of the solvent (water of alcohol) while it is related to the evaporation of the DMF solvent in the 150°C–200°C and the separation of water or any other solvent has created a strong bond with MOFs structures in the range of 250°C–300°C [23,26,35].

3.2. Adsorption tests

3.2.1. Evaluation of synthesized adsorbents performance

The performance of Cu-BTC, MIL-53(Al), and MIL-101(Cr) adsorbents in the process of removal of cobalt and manganese from synthesized wastewater is investigated and the results were compared with a commercial AC. The results are shown in Fig. 6. As observed in Fig. 6, the highest removal efficiency belongs to adsorbent MIL-101(Cr). The main reason for difference between adsorption rates of various adsorbents is related to the high surface area

of MIL-101(Cr). In addition, the removal rate of cobalt is higher than that of manganese in all the studied adsorbents, which indicates the proper agreement of adsorbent structure with cobalt ion. The functionalization of Cr-based MOF, MIL-101(Cr) by ED (ethylenediamine) is performed in three concentrations of 2, 5, and 10 mmol. The effect of various concentrations of ED on performance of MIL-101(Cr) adsorbent for removal of cobalt and manganese was shown in Fig. 7. The results revealed that the increased amount of ED increases the metal ion removal rate (up to 5 mmol concentration). This increase is due to that the one pair of electrons around amino groups of adsorbent can be shared with the 4d orbital of cobalt and manganese, thus increasing the amino groups result in increasing tendency of adsorption up to a certain point (10 mmol) [25]. On the contrary, increasing the ED concentration resulted in reduction in adsorption rate due to the reduction in the activated surface area of the adsorbents [14,25]. Hence, according to

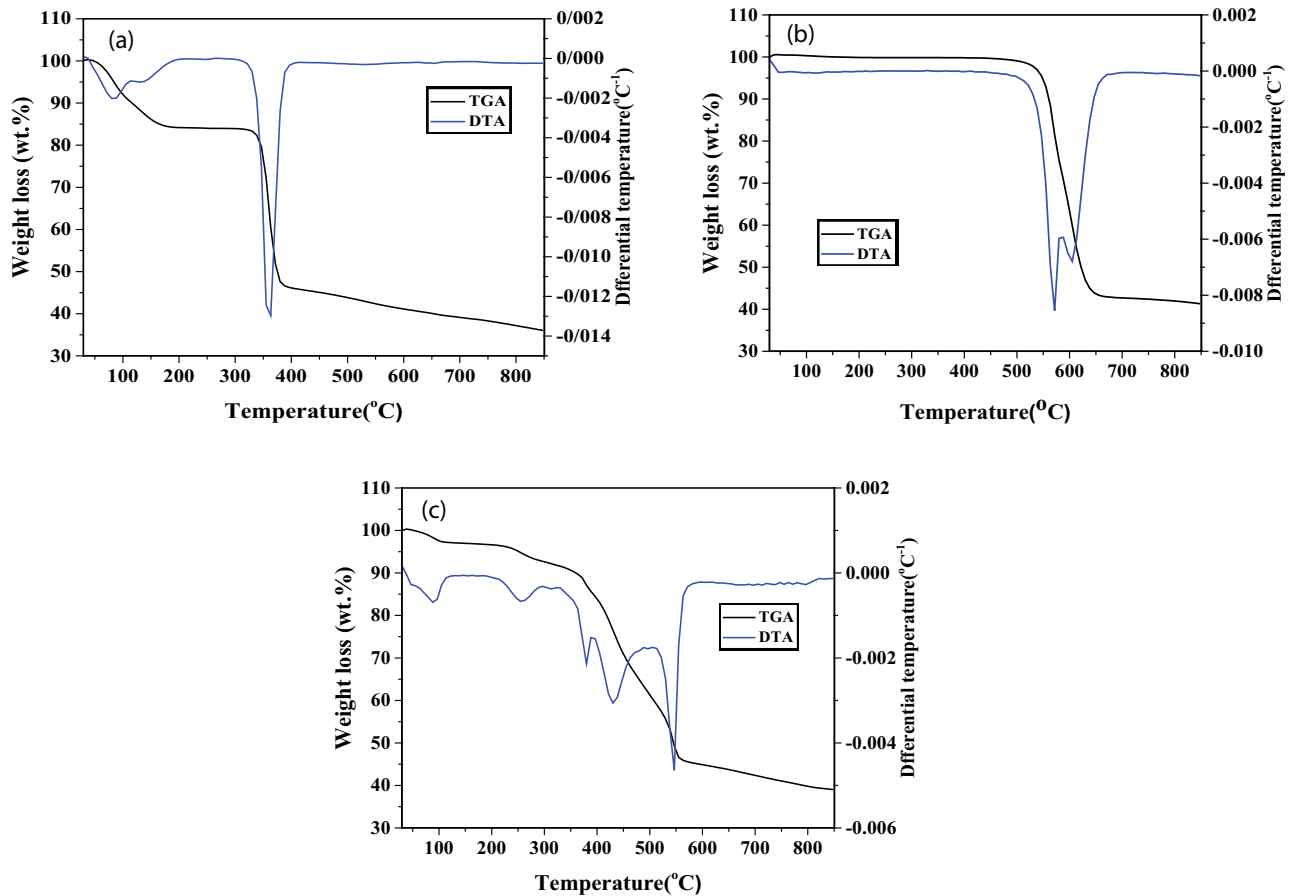


Fig. 5. DTA and TGA patterns of synthesized (a) Cu-BTC, (b) MIL-53(Al), and (c) MIL-101(Cr).

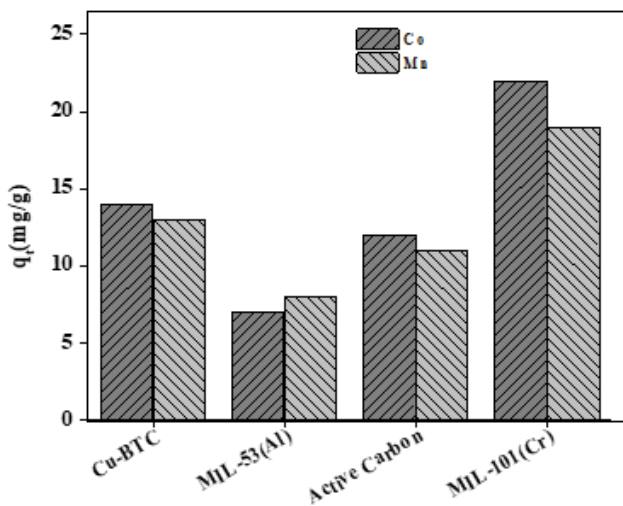


Fig. 6. Effect of different adsorbents on the removal of cobalt and manganese.

the results of the obtained efficiency, the 5 mmol concentration was selected as the superior concentration [25]. The separation percentage of the metal ions and the adsorption capacity of the modified adsorbent were calculated using the Eqs. (1) and (2).

3.2.2. FTIR spectra of functionalized adsorbents

Fig. 8 shows the results of FTIR spectra of MIL-101(Cr), ED-MIL-101 (2 mmol), ED-MIL-101 (5 mmol), and ED-MIL-101 (10 mmol). The peaks available in the range of 1,581 and 1,051 cm^{-1} can be assigned to N–H and C–N peaks, respectively. In addition, the peak available at the range 882 cm^{-1} is matched for $-\text{NH}_2$ [25]. Further, the increased density of peak intensity in the range of 3,221–3,434 cm^{-1} represents the increased number of N–H functionalized groups of the adsorbent [25,28].

3.3. Effect of important parameters for removal of cobalt and manganese by MIL-101-ED-5 (5 mmol) adsorbent

3.3.1. Effect of pH

Any change in pH of solution leads to a change in the zeta potential of adsorbent and the ionization degree of adsorbate and makes an adsorbent–adsorbate electrostatic interaction [15,28]. So, the solution pH affects the surface charge and the ionization degree as well as determining the kind of adsorbent. Based on the results shown in Fig. 9, increasing the pH from 3 to 6.5 results in increasing the removal rate of cobalt and manganese from 61.53% to 84.61% and 58.82% to 82.35%, respectively, at a 50 mg L^{-1} cobalt and manganese concentration and 0.02 g adsorbent.

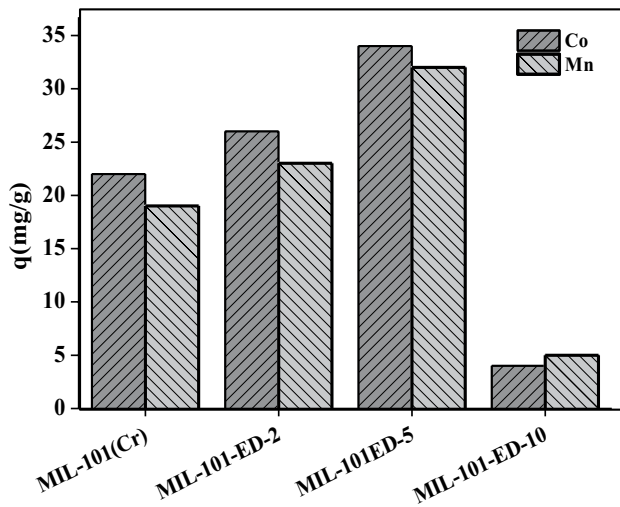


Fig. 7. Effect of various ED concentrations on performance of MIL-101(Cr) adsorbent for removal of cobalt and manganese.

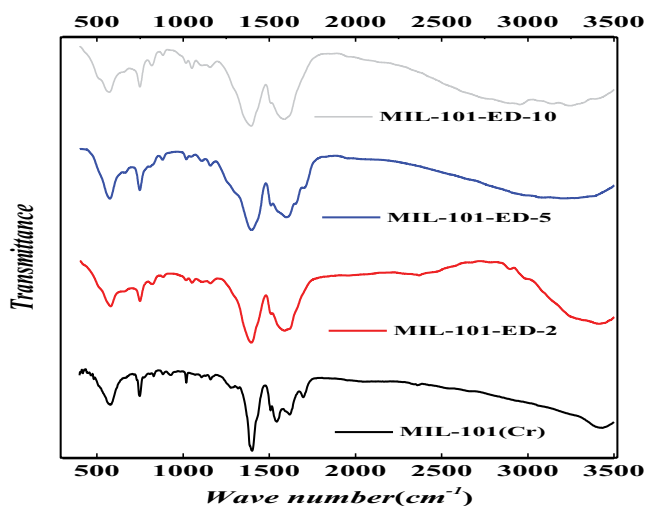


Fig. 8. FTIR spectra of functionalized adsorbents.

However, increasing the pH to more than 6.5 could reduce the adsorption rate of both metals, and at pH equal to 7, the minimum adsorption rate of cobalt and manganese was 76.93% and 74.51%, respectively. Therefore, pH of 6.5 was used as the optimal pH to perform the others of the experiment. It seems that pH reduction in acidic solutions leads to an increase in positive load (H^+) on adsorbent surface and accordingly activates the adsorbent surfaces. Therefore, the negative loads of adsorbate have more tendencies to be adsorbed on adsorbent surface and results in an increased adsorption rate. However, in solutions with $pH > 7$, there are more negative loads (OH^-) on adsorbent, leading to a repulsion between adsorbent and adsorbate and accordingly reduced adsorption [35–37]. The increase in cobalt adsorption rate due to increase in pH can be explained on the basis of the reduced competition between H^+ proton and metal cations in adsorbent functional groups as well as the reduced electrostatic discharge between adsorbent surfaces

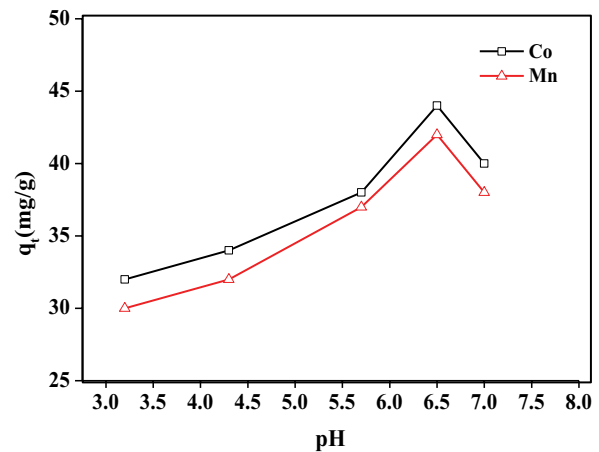


Fig. 9. Effect of pH on removal of cobalt and manganese (cobalt and manganese concentration, 50 mg L^{-1} ; adsorbent concentration of 0.02 g ; time of 240 min).

and metal ion. On the other hand, the increase in pH leads to the negative load (OH^-) on adsorbent surface, a repulsion between adsorbent and adsorbate, and accordingly reduced adsorption rate [20]. In the same study, Luo et al. [25] found that the maximum amount of adsorption rate of Pb was at $pH = 6$. They argued that when the solution has a pH less than 4, a huge amount of H^+ can be coordinated with MIL-101(Cr) ionized carboxyl and MIL-101-ED amino group. So, MIL-101(Cr) and MIL-101-ED (5 mmol) have a very low adsorption capacity at $pH < 4$. A solution with pH higher than 6 leads to a reduction in MIL-101(Cr) and MIL-101-ED (5 mmol), due to the higher amount of hydrolyzed ions produced compared with MIL-101(Cr) and MIL-101-ED (5 mmol). Hence, in order to achieve the best adsorption efficiency, the solution pH must be set at 6 [25].

3.3.2. Effect of contact time

The equilibrium adsorption time is one of the most important parameters of the kinetic process of adsorption because it helps to calculate the adsorption rate of adsorbate materials on adsorbent surface [10]. In order to study the adsorption time, various experimental tests were conducted between time 15 and 240 min, and other variables were kept constant. Fig. 10 illustrates the effect of time on removing of cobalt and manganese by MIL-101-ED-5 (5 mmol) and MIL-101-ED-2 (2 mmol). Normally, increasing of contact time leads to increase in the adsorption rate, due to the more opportunity of metal ions to make a bond with the adsorbent particles. Hence, the increased contact time between the adsorbent and the solution containing the metal ions leads to an increase in the metal ion adsorption by the adsorbent [36–38]. Such behavior is observed for both metal ions and both adsorbents between the contact times of 15–90 min. Also, the removal percentage of metal ions increases along with the duration time, and reaches to a constant rate after 90 min. It is worth noting that at the earliest time, the higher adsorption efficiency of cobalt and manganese are approximately close to each other while the adsorption efficiency of cobalt is clearly more than that of manganese by increasing

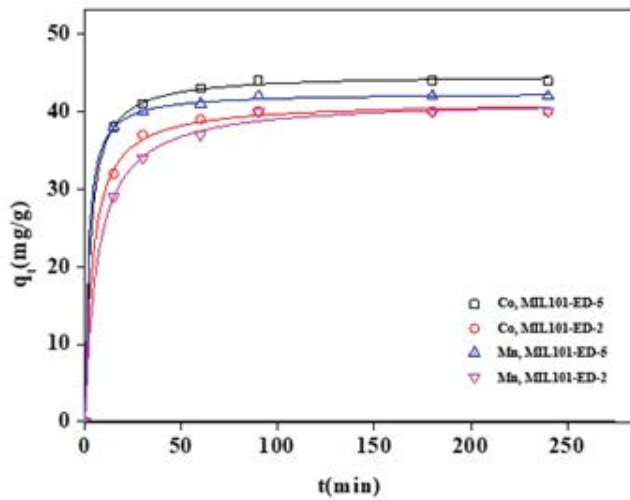


Fig. 10. Effect of contact time on removal of cobalt and manganese (adsorbate concentration of 50 mg L^{-1} , MIL-101-ED concentration of 0.02 g , $\text{pH} = 6.5$).

the contact time. Changshen Ye et al. [10] showed that the maximum adsorption of cobalt and manganese on Bentonite via adsorption was achieved during 60 min. The quick adsorption of these two heavy metals on sodium bentonite revealed that heavy metal ions adsorption from solution by bentonite is mainly due to chemical adsorption rather than physical adsorption [10].

3.3.3. Effect of initial concentration of cobalt and manganese

Different experiments with various concentrations of cobalt and manganese were conducted. As shown in Fig. 11, by increasing the initial concentration of metal ions, the adsorption percentage of adsorbent is decreased and the adsorption rate is increased. By increasing the initial concentration of metal ions, the number of ions competing to react with the functional groups of adsorbent surface increased

and accordingly the active sites of adsorbent became saturated [39]. In other words, the adsorption rate increased along with the increasing in the concentration of metal ions of the solution. In addition, increasing the concentration of metal ions lead to increasing the number of metal ions impact on the solution, which, in turn, accelerates the adsorption process [3,39].

3.3.4. Effect of temperature

Temperature has two important effects on adsorption process. First, increasing the temperature accelerates the penetration of the adsorbate molecules in internal and external layers of adsorbent cavities and also leading to a decrease in the viscosity of the solution. Second, the variation in the temperature affects the enthalpy and entropy of the adsorption process [40]. Before reaching the solution to equilibrium state, the increased temperature accelerates the adsorption process. Generally, by raising the temperature, the movement of molecules on the surface are increased and the single layers are not easily formed on the surface (less coating) result in decelerates of adsorption and increases of discharge [41]. The results of the effect of temperature on the adsorption are shown in Fig. 12. At concentration of 30 mg L^{-1} for cobalt and manganese and 0.02 g of adsorbent (MIL-101-ED-5), increasing the temperature from 25°C to 50°C would decrease the adsorption rate of cobalt and manganese from 90.32% to 9.67% and 87.33% to 6.67% , respectively. As shown in Fig. 12, increasing the temperature has a negative effect on the adsorption of both the metal ions. Hence, this adsorption process can be considered as an exothermic process, so the produced energy indicates the adsorption power. In addition, reducing the temperature improves the adsorption process due to exothermic process. Increase in the solution temperature leads to increase in the molecular movement of particles that results in weakening and sometimes break down of the bonds created between the adsorbed particles and adsorbent surface. Therefore, the pollutant particles adsorbed on the adsorbent surface will return to the soluble phase [41,42].

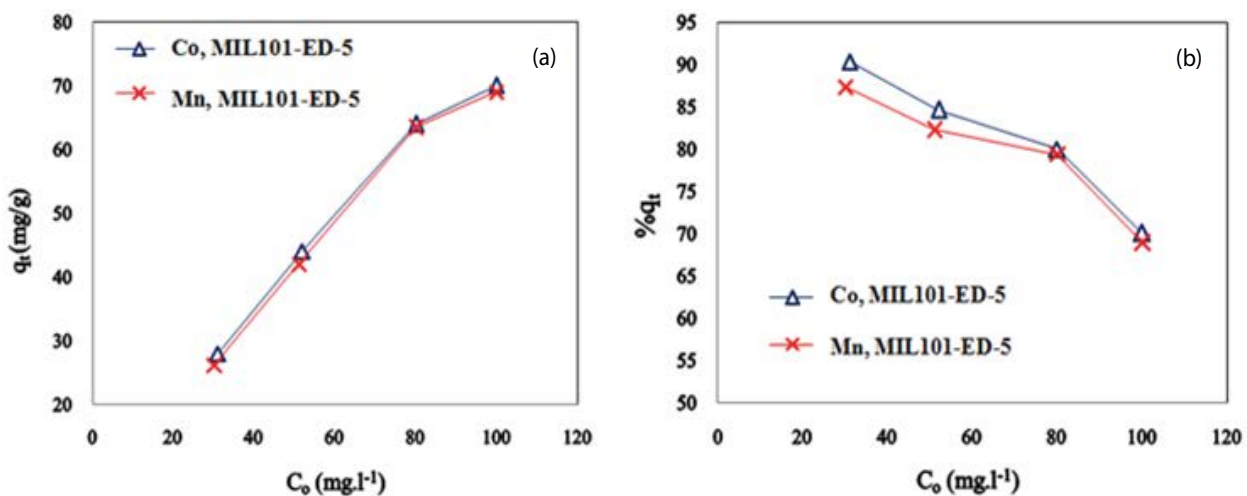


Fig. 11. Effect of changes in the initial concentrations of cobalt and manganese on (a) adsorption amount of CO and Mn and (b) separation percentage of CO and Mn at 25°C .

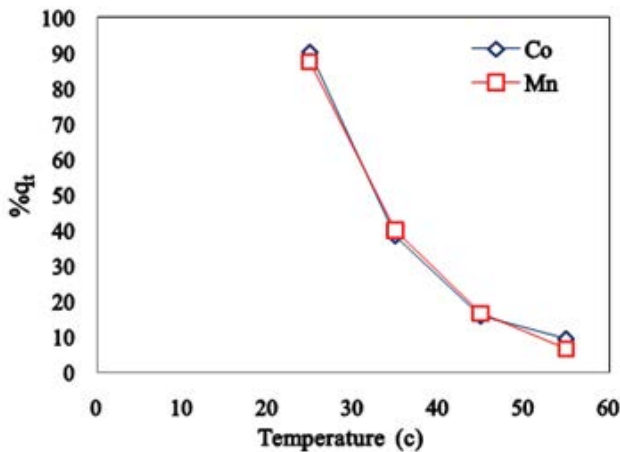


Fig. 12. Effect of temperature on removal of cobalt and manganese (concentration of cobalt and manganese 50 mg L⁻¹, contact time 90 min, adsorbent dose of 0.02 g).

3.3.5. Adsorption kinetics

In order to understand the dynamics of adsorption reactions of cobalt and manganese by adsorbents, the kinetic information of adsorption should be studied [17,26]. The dynamic adsorption data are shown in Fig. 13 and were treated with pseudo-first-order and pseudo-second-order kinetic models [17,26,43]. The pseudo-first-order model is expressed by the following equations:

$$\frac{dq_t}{dt} = k_1(q_e - q_t) \tag{3}$$

$$\ln(q_e - q_t) = \ln q_e - k_1 t \tag{4}$$

where q_t and q_e are the adsorbed amount of adsorbate (mg g⁻¹) at time t (min) and at equilibrium, respectively. k_1 is the pseudo-first-order kinetic constant (min⁻¹). Eq. (4) is derived from Eq. (3) by integrating subject to the initial

condition. The pseudo-first-order kinetics has been utilized for a variety of adsorption processes especially in water treatment [44,45]. The equilibrium adsorption capacity (q_e) and kinetic constant (k_1) were calculated from the intercept and slope of linear plots of $\ln(q_e - q_t)$ against t (Fig. 13a) and are reported in Table 4.

Dynamics of adsorption of Co and Mn can also be interpreted by pseudo-second-order kinetics [46,47] which is expressed by the following equations:

$$\frac{dq_t}{dt} = k_2(q_e - q_t)^2 \tag{5}$$

$$\frac{t}{q_t} = \frac{1}{k_2 q_e^2} + \frac{1}{q_e} t \tag{6}$$

where k_2 (g mg⁻¹ min⁻¹) is the pseudo-second-order rate constant. Eq. (6) is derived from Eq. (5) by integrating subject to the initial condition. Fig. 13b shows the linear plots of t/q_t against t for pseudo-second-order kinetic analysis of Co and Mn adsorption on MIL-101-ED (2 and 5 mmol) adsorbents. k_2 and q_e were calculated from the intercepts and slopes of these plots and are reported in Table 4. Comparison of the correlation coefficients (R^2) reported in Table 4 indicates that the adsorption kinetics is more adequately represented by a pseudo-second-order rather than a pseudo-first-order model. Furthermore, the values for maximum adsorption capacity (q_e) calculated from the pseudo-second-order model were in better agreement with that of the experimental values.

The dynamic adsorption data can be used also to identify the rate-controlling step in the adsorption process [46–48]. The three consecutive steps involved in the adsorption of an adsorbate by a porous adsorbent include: (I) transport of the adsorbate to the external surface of the adsorbent (film diffusion), (II) transport of the adsorbate within the pores of the adsorbent (intraparticle diffusion), and (III) adsorption of the adsorbate on the interface of the adsorbent. If the last step is fast enough, then the slowest transport portion

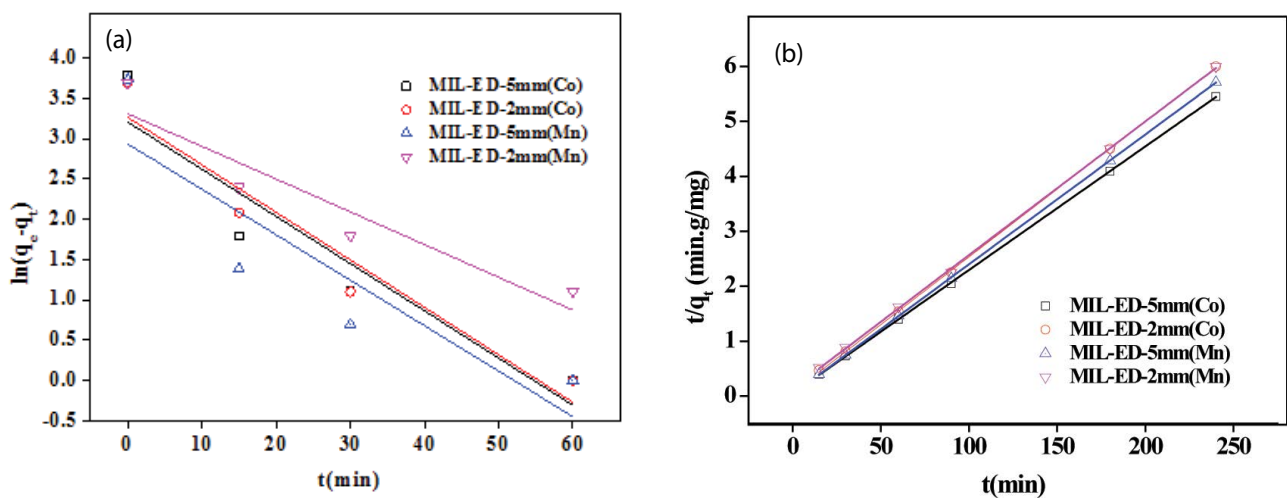


Fig. 13. First-order (a) and second-order (b) model plots for adsorption of Co and Mn on MIL-101-ED adsorbents.

Table 4
Determined kinetic model constants for the adsorption of cobalt and manganese

Adsorbate	C_0 (mg L ⁻¹)	Adsorbents	Pseudo-first-order kinetics			Pseudo-second-order kinetics			$q_{e,exp}$ (mg g ⁻¹)
			$q_{e,cal}$ (mg g ⁻¹)	k_1 (min ⁻¹)	R^2	$q_{e,cal}$ (mg g ⁻¹)	k_2 (g mg ⁻¹ min ⁻¹)	R^2	
Co	50	MIL-101-ED-5	24.6	0.0586	0.83	44.5	0.01064	0.99	44
		MIL-101-ED-2	26.2	0.0589	0.90	40.6	0.00882	0.99	40
Mn	50	MIL-101-ED-5	18.8	0.0564	0.69	42.3	0.01510	0.99	42
		MIL-101-ED-2	27.4	0.0406	0.84	41.1	0.00434	0.99	40

would determine the overall rate of adsorption [15,48]. The intraparticle diffusion model based on the theory proposed by Weber and Morris [49] would lead to the following equation:

$$q_t = k_d t^{0.5} + F \quad (7)$$

where q_t (mg g⁻¹) is the amount adsorbed at time t , k_d (mg g⁻¹ min^{-1/2}) is the intraparticle diffusion rate constant, and F (mg g⁻¹) is a constant related to the thickness of the boundary layer. If the value of F is zero, that is, the diffusion model plot of q_t against $t^{0.5}$ exhibits a straight line going through the origin, the adsorption process is only controlled by the intraparticle diffusion [48]. However, if the data exhibit multi-linear plot, then two or more steps influence the sorption process. The first sharper portion is the surface adsorption or instantaneous adsorption stage. The second portion is the gradual adsorption stage where intraparticle diffusion limits the rate of adsorption [33]. The diffusion model plot of Co and Mn adsorption on MIL-101(Cr)-ED (2 and 5 mmol) shown in Fig. 14 suggests a two-stage adsorption process; surface adsorption and intraparticle diffusion. The first linear portion of the plot is due to surface adsorption (faster step) while the second linear portion is due to the intraparticle diffusion within the pores of MIL-101(slower step) [15,47]. According to the results reported in Table 5, the values of the slope of slower portion (k_d) are not zero, which implies that the intraparticle diffusion controls the adsorption rate at the beginning. Furthermore, the intercept value (F) increased with increasing initial concentration of ED on MIL-101(Cr) suggesting that intraparticle diffusion is not the only rate-limiting step and that film diffusion also plays an important role in the adsorption of Co and Mn on MIL-101-ED [15,50]. According to Tables 4 and 5, second-order model satisfies the adsorption kinetics [51].

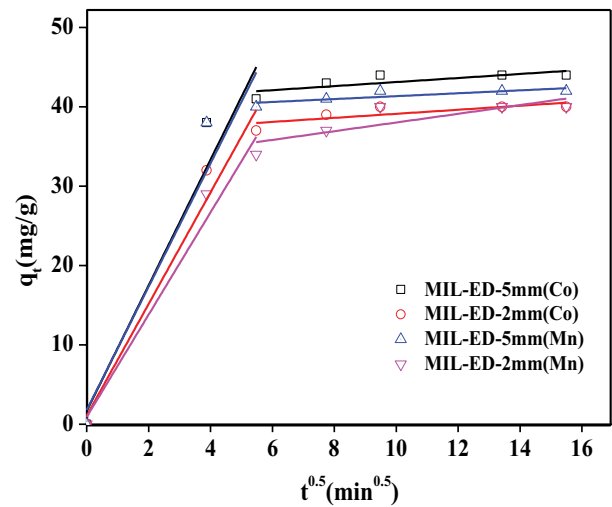


Fig. 14. Intraparticle diffusion model plot for absorption of Co and Mn on MIL-101-ED adsorbents.

3.3.6. Adsorption isotherms

Isotherm models turn the experimental results into the practical formulas with more useful parameters in order to be easily used for design or any scientific approaches. The plots of Langmuir [52], Freundlich [53,54], Temkin [55], and Redlich–Peterson (R-P) [56] isotherms were drawn using the non-linear form of their equations. Figs. 15 and 16 illustrated profiles of four isotherms at 25°C, for MIL-101-ED-5 (5 mmol), and constants of each model were calculated according to the linear model as shown in Table 6. The results of isotherms revealed that the correlation coefficients of Langmuir and R-P isotherms at 25°C are higher than that of others isotherms. The linear form of the Langmuir isotherm is given as:

Table 5
Kinetic parameters of intraparticle diffusion model for the adsorption of Co and Mn on MIL-101-ED (2 and 5 mmol)

Adsorbate	Adsorbent	C_0 (mg L ⁻¹)	Intraparticle diffusion rate		
			k_d (mg g ⁻¹ min ^{-1/2})	F	R^2
Co	MIL-101-ED-5	50	0.255	40.57	0.85
	MIL-101-ED-2	50	0.255	36.57	0.76
Mn	MIL-101-ED-5	50	0.183	39.51	0.87
	MIL-101-ED-2	50	0.548	32.54	0.76

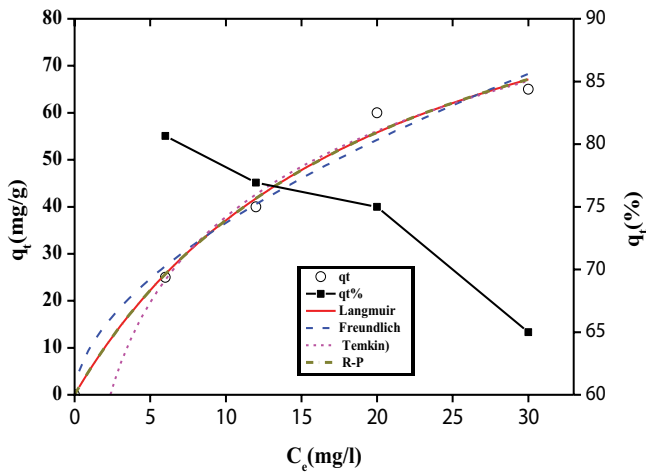


Fig. 15. Adsorption isotherms for adsorption of Co on MIL-101-ED-5 at 25°C.

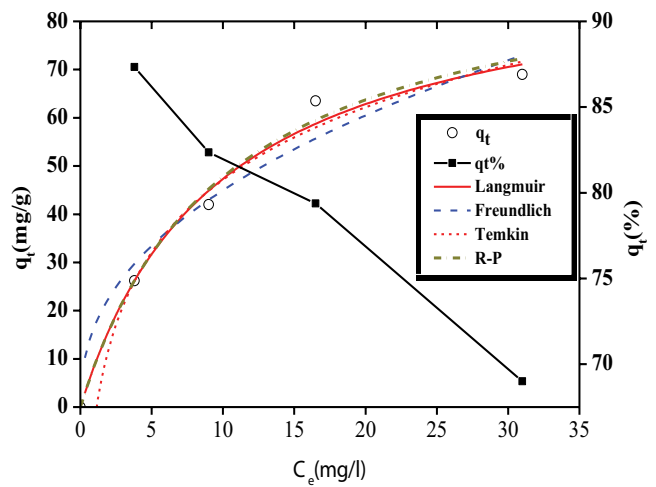


Fig. 16. Adsorption isotherms for adsorption of Mn on MIL-101-ED-5 at 25°C.

$$\frac{C_e}{q_e} = \frac{C_e}{q_{max}} + \frac{1}{q_{max}b} \tag{8}$$

where C_e (mg L^{-1}) is the equilibrium concentration of adsorbate, q_e (mg g^{-1}) is the amount of adsorbate adsorbed at equilibrium, q_{max} (mg g^{-1}) is the maximum adsorption capacity, and b (L mg^{-1}) is the Langmuir constant that indicates the adsorption tendency and it is regarded as the criteria of the adsorption power of molecules on the adsorbent. The higher values of b lead to more surface of the adsorbent covered by the molecules or the higher free energy of adsorption [26]. The values of b and q_{max} were calculated from the slope and intercept of linear plots of (C_e/q_e) against C_e for MIL-101(Cr)-ED (2 and 5 mmol) are reported in Table 6. Freundlich adsorption isotherm is a special case for heterogeneous surface energy in which the energy term in the Langmuir equation varies as a function of surface coverage and is not restricted to monolayer formation [57]. The linear form of the Freundlich equation is given by Eq. (9):

$$\ln q_e = \ln K_F + \left(\frac{1}{n}\right) \ln C_e \tag{9}$$

where C_e (mg L^{-1}) is the equilibrium concentration of adsorbate, q_e (mg g^{-1}) is the amount of adsorbate adsorbed at equilibrium state, K_F ($\text{mg g}^{-1}(\text{L/mg})^{-1/n}$) and $1/n$ represent the Freundlich constants corresponding to the adsorption capacity and adsorption intensity, respectively. The reversibility of adsorption process is indicated by n value. $1/n$ value is zero, the adsorption process is reversible, the value between zero and one shows an optimal process, and the value of more than 1 indicates an undesirable process, by continuation of which the adsorption process decreases and departs from the linear state [57,58]. The values of K_F and $1/n$ were calculated from the slope and intercept of linear plots of $\ln q_e$ against $\ln C_e$ and are reported in Table 6. Due to proximity of correlation coefficients for the Langmuir and Freundlich models, Redlich–Peterson (R-P) was used as an adsorption isotherm to confirm the obtained results. The Redlich–Peterson isotherm amends the inaccuracies of two parameter Langmuir and Freundlich isotherms in most adsorption systems. This model is a hybrid isotherm featuring both Langmuir and Freundlich isotherms which incorporates three parameters into an empirical equation as follows [23,58]:

Table 6
Equilibrium parameters for Co and Mn adsorption over MIL-101-ED-2 and 5 mmol at $T = 25^\circ\text{C}$

Adsorbate	Adsorbents	Langmuir parameters			Freundlich parameters			Redlich–Peterson model				Temkin parameters		
		q_{max} (mg g^{-1})	b (L mg^{-1})	R^2	K_F (mg g^{-1}) ($\text{L/mg}^{-1/n}$)	$1/n$	R^2	a_R (L mg^{-1}) $^\beta$	K_R (L g^{-1})	β	R^2	A (L g^{-1})	B (J mol^{-1})	R^2
Cobalt	MIL-101-ED-5 (5 mmol)	87.2	0.146	0.97	20.28	0.38	0.92	0.132	12.36	1	0.97	1.41	19.22	0.91
	MIL-101-ED-2 (2 mmol)	112.4	0.049	0.96	9.90	0.57	0.96	0.493	5.54	1	0.98	0.42	26.29	0.95
Manganese	MIL-101-ED-5 (5 mmol)	93.4	0.103	0.97	16.8	0.43	0.93	0.104	9.53	1	0.98	0.88	21.68	0.92
	MIL-101-ED-2 (2 mmol)	104.9	0.055	0.99	10.64	0.53	0.95	0.055	5.75	1	0.99	0.46	24.86	0.94

$$q_e = \frac{K_R C_e}{1 + a_R C_e^\beta} \quad (10)$$

where K_R ($L g^{-1}$) and a_R ($L mg^{-1}$) $^\beta$ are the Redlich–Peterson isotherm constants and β is R-P isotherm exponent. The model has a linear dependence on concentration in the numerator and an exponential function in the denominator to represent adsorption equilibria over a wide concentration range, that can be applied either in homogeneous or heterogeneous systems due to its versatility [23,59]. Typically, a minimization procedure is adapted to solving the equation by maximizing the correlation coefficient between the experimental data points and theoretical model predictions. In the limit, it approaches the Freundlich isotherm model at high concentrations (as the exponent β tends to zero) and is in accordance with the low concentration limit of the ideal Langmuir model (as the β values are all close to one) [58,59]. The results obtained from R-P equation are also presented in Table 6. By comparing the values of R^2 , the Langmuir isotherm gave a better fit of the adsorption data compared with

the Freundlich isotherm. However, the Redlich–Peterson model was shown to be an improved fit for both Co and Mn. As shown in Table 6, the exponent β of the R-P model for Co and Mn over MIL-101-ED was obtained as 1 by the minimization algorithm confirming that the Langmuir isotherm (monolayer adsorption mechanism) is more adequate [23].

3.3.7. Thermodynamics of adsorption

In order to perform a precise study on the effect of temperature on adsorption rate, some thermodynamic experiments were conducted under adsorbent dosage of 0.02 g, pH of 6.5, initial concentration of cobalt and manganese of 30 mg L⁻¹, and different temperatures 25°C, 35°C, 40°C, and 50°C. Figs. 17a–d illustrate the plots of thermodynamic changes of Co and Mn adsorption over MIL-101-ED-5 and the results are presented in Table 7. The negative values of ΔG at all temperatures imply that the adsorption proceeds spontaneously [35]. The negative value of ΔH is another evidence of exothermic adsorption process. In addition,

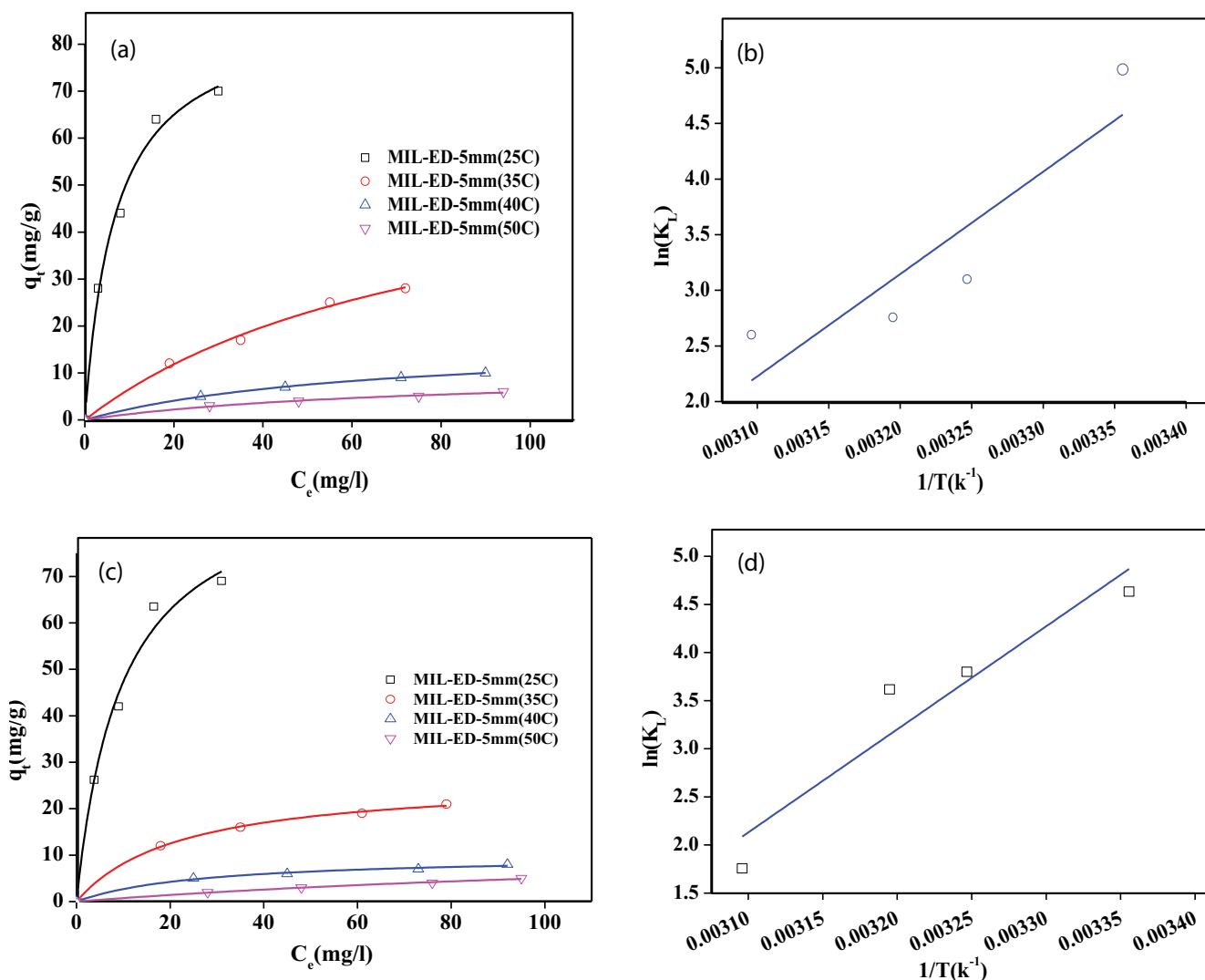


Fig. 17. Thermodynamic plots for cobalt ((a) and (b)) and manganese ((c) and (d)) adsorption over MIL-101-ED-5 (5 mmol).

Table 7

Thermodynamic parameters for adsorption of cobalt and manganese ions using MIL-101-ED adsorbent (5 mmol)

Adsorbate	Temperature (°C)	b (L mg ⁻¹)	q_{\max} (mg g ⁻¹)	R^2	ΔG (kJ mol ⁻¹)	ΔH (kJ mol ⁻¹)	ΔS (J mol ⁻¹ K ⁻¹)
Co	25	0.146	87.2	0.97	-12.35	-76.53	-218.7
	35	0.022	60.3	0.98	-0.90		
	40	0.016	17.0	0.99	-0.92		
	50	0.014	10.4	0.96	-1.08		
Mn	25	0.103	93.4	0.97	-11.48	-89.01	-258.2
	35	0.045	26.5	0.98	-1.11		
	40	0.037	9.94	0.99	-1.2		
	50	0.006	13.7	0.97	-0.73		

negative value of ΔS represents the increased tendency of MIL-101-ED-5 to adsorb Co and Mn metal ions vs. desorption, which in turn leads to the spontaneity of the process due to its high exothermic process [35,60].

4. Conclusion

The liquid-phase adsorption of Co and Mn has been studied using MOFs Cu-BTC, MIL-53(Al), MIL-101(Cr), AC, and also MIL-101 functionalized with 2, 5, and 10 mmol ED as adsorbent. The high adsorption capacity of MIL-101-ED-5 for cobalt and manganese was obtained due to its high porosity, surface area, and an optimum amount of ED as amino group. According to the results, the maximum capacity to remove these two hazardous metal ions was obtained at pH = 6.5, temperature = 25°C, cobalt and manganese concentration of 30 mg L⁻¹ and the adsorption process reaches equilibrium during 90 min. In addition, the maximum efficiency of the functionalized adsorbent process was obtained at 5 mmol concentration of ED, leading to a reverse result due to further increase (10 mmol). In fact, the increase in ED creates a change in the morphology of the synthesized adsorbent and reduces the active surface of adsorbent and accordingly the adsorption rate. By applying these conditions, the maximum percentage of cobalt and manganese adsorption by the functionalized adsorbent in the adsorption process is equal to 90.32% and 87.33%, respectively. The dynamic adsorption data were well fitted with a pseudo-second-order kinetic model. The equilibrium adsorption isotherms were adequately described by the Langmuir model. Finally, the functionalized adsorbent MIL-101-ED-5 showed an acceptable and higher adsorption capacity for removal of hazardous heavy metals same as cobalt and manganese.

Acknowledgment

The authors gratefully acknowledge the financial support provided by Islamic Azad University of Mahshahr branch, Iran.

References

- [1] A. Dąbrowski, Z. Hubicki, P. Podkościelny, E. Robens, Selective removal of the heavy metal ions from waters and industrial wastewaters by ion-exchange method, *Chemosphere*, 56 (2004) 91–106.
- [2] A.N. Vasiliev, L.V. Golovko, V.V. Trachevsky, G.S. Hall, J.G. Khinast, Adsorption of heavy metal cations by organic ligands grafted on porous materials, *Microporous Mesoporous Mater.*, 118 (2009) 251–257.
- [3] F. Fu, Q. Wang, Removal of heavy metal ions from wastewaters: a review, *J. Environ. Manage.*, 92 (2011) 407–418.
- [4] M.M. Matlock, B.S. Howerton, D.A. Atwood, Chemical precipitation of heavy metals from acid mine drainage, *Water Res.*, 36 (2002) 4757–4764.
- [5] H. Ozaki, K. Sharma, W. Saktaywin, Performance of an ultra-low-pressure reverse osmosis membrane (ULPROM) for separating heavy metal: effects of interference parameters, *Desalination*, 144 (2002) 287–294.
- [6] E. Erdem, N. Karapinar, R. Donat, The removal of heavy metal cations by natural zeolites, *J. Colloid Interface Sci.*, 280 (2004) 309–314.
- [7] E. Bazrafshan, A.H. Mahvi, S. Naseri, A.R. Mesdaghinia, Performance evaluation of electrocoagulation process for removal of chromium (VI) from synthetic chromium solutions using iron and aluminum electrodes, *Turk. J. Eng. Environ. Sci.*, 32 (2008) 59–66.
- [8] M.A. Habib, S.M.R.A. Moghaddam, M. Arami, S.H. Hashemi, Optimization of the electrocoagulation process for removal of Cr (VI) using Taguchi method, *J. Water Wastewater*, 22 (2012) 22–24.
- [9] A.-H. Chen, S.-C. Liu, C.-Y. Chen, C.-Y. Chen, Comparative adsorption of Cu(II), Zn(II), and Pb(II) ions in aqueous solution on the crosslinked chitosan with epichlorohydrin, *J. Hazard. Mater.*, 154 (2008) 184–191.
- [10] C. Ye, M. Lin, Z. Qi, W. Zhu, C. Yang, T. Qiu, Adsorption of Co(II) and Mn(II) ions from pure terephthalic acid wastewater onto Na-bentonite, *Desal. Wat. Treat.*, 57 (2016) 20856–20866.
- [11] T.M. Florence, Electrochemical approaches to trace element speciation in waters: a review, *Analyst*, 111 (1986) 489–505.
- [12] A. Fujishima, Electrochemical photolysis of water at a semiconductor electrode, *Nature*, 238 (1972) 37–38.
- [13] J. Kumpiene, A. Lagerkvist, C. Maurice, Stabilization of As, Cr, Cu, Pb and Zn in soil using amendments – a review, *Waste Manage.*, 28 (2008) 215–225.
- [14] F. Ke, L.-G. Qiu, Y.-P. Yuan, F.-M. Peng, X. Jiang, A.-J. Xie, Y.-H. Shen, J.-F. Zhu, Thiol-functionalization of metal-organic framework by a facile coordination-based postsynthetic strategy and enhanced removal of Hg²⁺ from water, *J. Hazard. Mater.*, 196 (2011) 36–43.
- [15] A. Behvandi, A. Safekordi, F. Khorasheh, Removal of benzoic acid from industrial wastewater using metal organic frameworks: equilibrium, kinetic and thermodynamic study, *J. Porous Mater.*, 24 (2017) 165–178.
- [16] S. Tian, P. Jiang, P. Ning, Y. Su, Enhanced adsorption removal of phosphate from water by mixed lanthanum/aluminum pillared montmorillonite, *Chem. Eng. J.*, 151 (2009) 141–148.
- [17] Z. Zhao, X. Li, Z. Li, Adsorption equilibrium and kinetics of p-xylene on chromium-based metal organic framework MIL-101, *Chem. Eng. J.*, 173 (2011) 150–157.

- [18] H. Furukawa, K.E. Cordova, M. O'Keeffe, O.M. Yaghi, The chemistry and applications of metal-organic frameworks, *Science*, 341 (2013) 1230444.
- [19] U. Mueller, M. Schubert, F. Teich, H. Puetter, K. Schierle-Arndt, J. Pastre, Metal-organic frameworks—prospective industrial applications, *J. Mater. Chem.*, 16 (2006) 626–636.
- [20] R.J. Kuppler, D.J. Timmons, Q.-R. Fang, J.-R. Li, T.A. Makal, M.D. Young, D. Yuan, D. Zhao, W. Zhuang, H.-C. Zhou, Potential applications of metal-organic frameworks, *Coord. Chem. Rev.*, 253 (2009) 3042–3066.
- [21] M. Asgher, H.N. Bhatti, Evaluation of thermodynamics and effect of chemical treatments on sorption potential of *Citrus* waste biomass for removal of anionic dyes from aqueous solutions, *Ecol. Eng.*, 38 (2012) 79–85.
- [22] A. Vishnyakov, P.I. Ravikovitch, A.V. Neimark, M. Bülow, Q.M. Wang, Nanopore structure and sorption properties of Cu-BTC metal-organic framework, *Nano Lett.*, 3 (2003) 713–718.
- [23] A. Behvandia, F. Khorashehb, A.A. Safekordia, Adsorption of terephthalic acid and *p*-toluic acid from aqueous solution using metal organic frameworks: effect of molecular properties of the adsorbates and structural characteristics of the adsorbents, *Desal. Wat. Treat.*, 66 (2017) 367–382.
- [24] L. Hamon, C. Serre, T. Devic, T. Loiseau, F. Millange, G. Férey, G.D. Weireld, Comparative study of hydrogen sulfide adsorption in the MIL-53(Al, Cr, Fe), MIL-47(V), MIL-100(Cr), and MIL-101(Cr) metal-organic frameworks at room temperature, *J. Am. Chem. Soc.*, 131 (2009) 8775–8777.
- [25] X. Luo, L. Ding, J. Luo, Adsorptive removal of Pb(II) ions from aqueous samples with amino-functionalization of metal-organic frameworks MIL-101(Cr), *J. Chem. Eng. Data*, 60 (2015) 1732–1743.
- [26] C. Chen, M. Zhang, Q. Guan, W. Li, Kinetic and thermodynamic studies on the adsorption of xylenol orange onto MIL-101(Cr), *Chem. Eng. J.*, 183 (2012) 60–67.
- [27] Y. Hete, S. Gholase, R. Khope, Adsorption study of cobalt on treated granular activated carbon, *E-J. Chem.*, 9 (2012) 335–339.
- [28] K. Yang, Q. Sun, F. Xue, D. Lin, Adsorption of volatile organic compounds by metal-organic frameworks MIL-101: influence of molecular size and shape, *J. Hazard. Mater.*, 195 (2011) 124–131.
- [29] O. Lebedev, F. Millange, C. Serre, G. Van Tendeloo, G. Férey, First direct imaging of giant pores of the metal-organic framework MIL-101, *Chem. Mater.*, 17 (2005) 6525–6527.
- [30] J. Yang, Q. Zhao, J. Li, J. Dong, Synthesis of metal-organic framework MIL-101 in TMAOH-Cr(NO₃)₃-H₂BDC-H₂O and its hydrogen-storage behavior, *Microporous Mesoporous Mater.*, 130 (2010) 174–179.
- [31] C.-X. Yang, H.-B. Ren, X.-P. Yan, Fluorescent metal-organic framework MIL-53(Al) for highly selective and sensitive detection of Fe³⁺ in aqueous solution, *Anal. Chem.*, 85 (2013) 7441–7446.
- [32] B.D. Chandler, D.T. Cramb, G.K. Shimizu, Microporous metal-organic frameworks formed in a stepwise manner from luminescent building blocks, *J. Am. Chem. Soc.*, 128 (2006) 10403–10412.
- [33] C.B. Vidal, A.L. Barros, C.P. Moura, A.C. De Lima, F.S. Dias, L.C. Vasconcellos, P.B. Fachine, R.F. Nascimento, Adsorption of polycyclic aromatic hydrocarbons from aqueous solutions by modified periodic mesoporous organosilica, *J. Colloid Interface Sci.*, 357 (2011) 466–473.
- [34] P. Rallapalli, D. Patil, K. Prasanth, R.S. Somani, R. Jasra, H. Bajaj, An alternative activation method for the enhancement of methane storage capacity of nanoporous aluminium terephthalate, MIL-53(Al), *J. Porous Mater.*, 17 (2010) 523–528.
- [35] E. Haque, J.E. Lee, I.T. Jang, Y.K. Hwang, J.-S. Chang, J. Jegal, S.H. Jhung, Adsorptive removal of methyl orange from aqueous solution with metal-organic frameworks, porous chromium-benzenedicarboxylates, *J. Hazard. Mater.*, 181 (2010) 535–542.
- [36] Q. Du, J. Sun, Y. Li, X. Yang, X. Wang, Z. Wang, L. Xia, Highly enhanced adsorption of congo red onto graphene oxide/chitosan fibers by wet-chemical etching off silica nanoparticles, *Chem. Eng. J.*, 245 (2014) 99–106.
- [37] O. Amuda, A. Giwa, I. Bello, Removal of heavy metal from industrial wastewater using modified activated coconut shell carbon, *Biochem. Eng. J.*, 36 (2007) 174–181.
- [38] A.K. Meena, G. Mishra, P. Rai, C. Rajagopal, P. Nagar, Removal of heavy metal ions from aqueous solutions using carbon aerogel as an adsorbent, *J. Hazard. Mater.*, 122 (2005) 161–170.
- [39] F. Ge, M.-M. Li, H. Ye, B.-X. Zhao, Effective removal of heavy metal ions Cd²⁺, Zn²⁺, Pb²⁺, Cu²⁺ from aqueous solution by polymer-modified magnetic nanoparticles, *J. Hazard. Mater.*, 211 (2012) 366–372.
- [40] S. Babel, T.A. Kurniawan, Low-cost adsorbents for heavy metals uptake from contaminated water: a review, *J. Hazard. Mater.*, 97 (2003) 219–243.
- [41] F. Gode, E. Pehlivan, Removal of chromium(III) from aqueous solutions using Lewatit S 100: the effect of pH, time, metal concentration and temperature, *J. Hazard. Mater.*, 136 (2006) 330–337.
- [42] Å. Fritioff, L. Kautsky, M. Greger, Influence of temperature and salinity on heavy metal uptake by submersed plants, *Environ. Pollut.*, 133 (2005) 265–274.
- [43] D.L. Guerra, C. Airoidi, V.P. Lemos, R.S. Angélica, Adsorptive, thermodynamic and kinetic performances of Al/Ti and Al/Zr-pillared clays from the Brazilian Amazon region for zinc cation removal, *J. Hazard. Mater.*, 155 (2008) 230–242.
- [44] H. Zheng, D. Liu, Y. Zheng, S. Liang, Z. Liu, Sorption isotherm and kinetic modeling of aniline on Cr-bentonite, *J. Hazard. Mater.*, 167 (2009) 141–147.
- [45] V. Dang, H. Doan, T. Dang-Vu, A. Lohi, Equilibrium and kinetics of biosorption of cadmium(II) and copper(II) ions by wheat straw, *Bioresour. Technol.*, 100 (2009) 211–219.
- [46] N.A. Khan, S.H. Jhung, Remarkable Adsorption Capacity of CuCl₂-Loaded Porous Vanadium Benzenedicarboxylate for Benzothiophene, *Angew. Chem.*, 124 (2012) 1224–1227.
- [47] R. Arasteh, M. Masoumi, A. Rashidi, L. Moradi, V. Samimi, S. Mostafavi, Adsorption of 2-nitrophenol by multi-wall carbon nanotubes from aqueous solutions, *Appl. Surf. Sci.*, 256 (2010) 4447–4455.
- [48] F. Leng, W. Wang, X.J. Zhao, X.L. Hu, Y.F. Li, Adsorption interaction between a metal-organic framework of chromium-benzenedicarboxylates and uranine in aqueous solution, *Colloids Surf., A*, 441 (2014) 164–169.
- [49] T.W. Weber, R.K. Chakravorti, Pore and solid diffusion models for fixed-bed adsorbents, *AIChE J.*, 20 (1974) 228–238.
- [50] L. Xie, D. Liu, H. Huang, Q. Yang, C. Zhong, Efficient capture of nitrobenzene from waste water using metal-organic frameworks, *Chem. Eng. J.*, 246 (2014) 142–149.
- [51] A.C.A. de Lima, R.F. Nascimento, F.F. de Sousa, M. Josue Filho, A.C. Oliveira, Modified coconut shell fibers: a green and economical sorbent for the removal of anions from aqueous solutions, *Chem. Eng. J.*, 185–186 (2012) 274–284.
- [52] I. Langmuir, The constitution and fundamental properties of solids and liquids. Part I. Solids, *J. Am. Chem. Soc.*, 38 (1916) 2221–2295.
- [53] O. Altın, H.Ö. Özbelge, T. Doğu, Use of general purpose adsorption isotherms for heavy metal-clay mineral interactions, *J. Colloid Interface Sci.*, 198 (1998) 130–140.
- [54] H. Freundlich, Über die adsorption in losungen [Adsorption in solution], *Z. Phys. Chem.*, 57 (1906) 385–490.
- [55] M. Temkin, V. Pyzhev, Kinetics of ammonia synthesis on promoted iron catalysts, *Acta Physicochim Urs*, 12 (1940) 217–222.
- [56] O. Redlich, D.L. Peterson, A useful adsorption isotherm, *J. Phys. Chem.*, 63 (1959) 1024–1024.
- [57] A. Dada, A. Olalekan, A. Olatunya, O. Dada, Langmuir, Freundlich, Temkin and Dubinin-Radushkevich isotherms studies of equilibrium sorption of Zn²⁺ unto phosphoric acid modified rice husk, *IOSR J. Appl. Chem.*, 3 (2012) 38–45.
- [58] K.Y. Foo, B.H. Hameed, Insights into the modeling of adsorption isotherm systems, *Chem. Eng. J.*, 156 (2010) 2–10.
- [59] M. Ahmaruzzaman, D. Sharma, Adsorption of phenols from wastewater, *J. Colloid Interface Sci.*, 287 (2005) 14–24.
- [60] K. Chai, H. Ji, Dual functional adsorption of benzoic acid from wastewater by biological-based chitosan grafted β-cyclodextrin, *Chem. Eng. J.*, 203 (2012) 309–318.